

**NASA  
Technical  
Paper  
2744**

1987

# Hydrogen Trapping and the Interaction of Hydrogen With Metals

Merlin D. Danford

*George C. Marshall Space Flight Center  
Marshall Space Flight Center, Alabama*

**NASA**

National Aeronautics  
and Space Administration

Scientific and Technical  
Information Office

## **ACKNOWLEDGMENTS**

The author wishes to thank Mrs. Pat Johnson for the hydrogen determinations with the Leco Analyzer, Mrs. Dinah Higgins for the X-ray diffraction work, and Mr. Wendell DeWeese for the metallographic work. Their contributions are greatly appreciated.

## TABLE OF CONTENTS

	Page
INTRODUCTION.....	1
ANALYTICAL TREATMENT OF DIFFUSION EQUATIONS.....	1
Hydrogen Absorption by Cylinders.....	1
Hydrogen Desorption from Cylinders.....	2
NUMERICAL SOLUTION WITH PDEONE.....	4
EXPERIMENTAL.....	6
RESULTS AND DISCUSSION.....	7
General.....	7
Hydrogen Trapping and Metal Embrittlement.....	8
The Entry of Hydrogen into BCC Metals.....	9
The Interaction of Hydrogen with Metals.....	9
CONCLUSIONS.....	10
REFERENCES.....	12

## LIST OF ILLUSTRATIONS

Figure	Title	Page
1.	Desorption profiles for Incoloy 903 cylinders .....	13
2.	Exploded view of the sample holder .....	14
3.	Theoretical and experimental desorption curves for an Incoloy 903 cylinder charged at 25°C.....	15
4.	Theoretical and experimental desorption curves for an 18 Ni (250) maraging steel cylinder charged at 150°C.....	16
5.	Theoretical and experimental desorption curves for an 18 Ni (250) maraging steel cylinder charged at 25°C.....	17
6.	Theoretical absorption profiles for 4340 (6414) and Incoloy 903 cylinders charged at 25°C .....	18
7.	Least squares fit of observed hydrogen distribution with diffusion equation for an Incoloy 903 cylinder charged at 150°C .....	19
8.	The hypothetical structure of NiH (NaCl structure). Positions of H atoms are designated by open circles.....	20
9.	The hypothetical structure of Fe <sub>2</sub> H <sub>3</sub> (Perovskite structure). Positions of H atoms are designated by open circles .....	21

## LIST OF TABLES

Table	Title	Page
1.	Values of $\beta$ and $\text{Log } \alpha$ Obtained by Least Squares Fit of Observed Data.....	22
2.	Hydrogen Concentrations in Metals Charged Electrolytically at 25°C and 150°C.....	23
3.	Hydrogen Distribution Uniformities in Cylinders Charged at 25°C.....	24
4.	Structure Types and Unit Cell Parameters for Metal Alloys.....	25
5.	Hydrogen Distribution Uniformities in Cylinders Charged at 150°C.....	
6.	Values of Diffusion Coefficients Obtained for Various Alloys .....	26
7.	Values of $D_0$ and $E$ for the Arrhenius Equation, $D = D_0 \exp (-E/RT)$ .....	27
8.	Relation of Hydrogen Trapping to Titanium Content and Temperature .....	
9.	Values of $C_0$ , Rate Constant and Half-Life Obtained on Baking at 430°F .....	28

## TECHNICAL PAPER

# HYDROGEN TRAPPING AND THE INTERACTION OF HYDROGEN WITH METALS

## INTRODUCTION

This study is a part of a broad program aimed toward an understanding of the nature of hydrogen embrittlement. Such knowledge is important for the proper treatment of problems involving hydrogen effects in the high strength metals employed in the Space Shuttle Main Engine. A previous study in this connection was carried out with flat metal specimens and involved the electrochemical method only [1]. The present work involves both the electrochemical method and hydrogen analysis using the fusion technique, wherein the total hydrogen concentration can be obtained. Only the diffusible or mobile hydrogen can be determined using the electrochemical method. Therefore, by using both methods, concentrations of trapped hydrogen can be obtained through the differences in concentrations obtained with each method.

In addition, a sensitive check on the validity and power of the electrochemical method can be obtained through use of both techniques. Where hydrogen trapping is not a factor, the agreement of observed concentrations obtained using both methods provides a sensitive check on the validity and accuracy of the electrochemical method. It will be shown in one of the following sections that the hydrogen diffusion coefficient ( $D$ ) in the metal, obtained with the electrochemical method, is also intimately associated with the value of hydrogen concentration ( $C_0$ ) obtained, so that the fusion analysis also provides verification of the value of  $D$  obtained with the electrochemical method.

In order to properly use both methods, recourse was made to the use of cylindrical specimens. Computer methods were developed for analysis of the data obtained with the electrochemical method. Both the exact analytical solutions to the diffusion equations for cylinders, as given by Barrer [2], and numerical methods, as used by the computer program PDEONE [3], were developed, but comparison by the two methods for cylindrical specimens indicated that the numerical method gave smoother curves although the results agreed very well. As a result, it was used exclusively for the analysis of the electrochemical desorption data obtained in the present work.

## ANALYTICAL TREATMENT OF DIFFUSION EQUATIONS

### Hydrogen Absorption by Cylinders

In the case of absorption by a circular cylinder of radius  $r = a$  where a constant surface concentration  $S$  is maintained and the medium is initially free of solute, the solution to the diffusion equation for radial flow may be given in terms of Bessel's function of the first kind and of zero order  $J_0(X)$  and its differential  $J_0'(X)$ . The solution is, for a given charge time  $t$  and diffusion coefficient  $D$ ,

$$f(r) = S \left( 1 + \frac{2}{a} \sum_1^{\infty} \frac{1}{\alpha_n} \frac{J_0(\alpha_n r)}{J_0'(\alpha_n a)} e^{-D\alpha_n^2 t} \right) \quad (1)$$

where  $\alpha_n$  is the nth root of the equation  $J_0(\alpha_n a) = 0$ . The first 2 roots of  $J_0(\alpha_n a) = 0$  are

$$\alpha_1 = \frac{2.405}{a}, \quad \alpha_2 = \frac{5.520}{a} \quad (2)$$

In the present case, a total of eight such roots were used, this number being adequate to express the diffusion process. The functions  $J_0(X)$  and  $J_0'(X)$  are given by the series

$$J_0(X) = 1 - (1/2X)^2 + \frac{(1/2X)^4}{1 \cdot 2^2} - \frac{(1/2X)^6}{1 \cdot 2^2 \cdot 3^2} + \dots \quad (3)$$

$$J_0'(X) = -(1/2X) + \frac{(1/2X)^3}{1 \cdot 2} - \frac{(1/2X)^5}{1 \cdot 2^2 \cdot 3} + \dots \quad (4)$$

and their values for any values of X are given in tables. The mean or observed hydrogen concentration in the cylinder is given by

$$C = \frac{2}{a^2} \int_0^a f(r) r dr \quad (5)$$

In practice, the value of S, the apparent surface concentration of hydrogen, is determined by dividing the observed hydrogen concentration, which is also the mean concentration, by the value of C obtained by equation (5), which is calculated assuming unit values of S in equation (1) for the calculation of  $f(r)$ .

### Hydrogen Desorption from Cylinders

The treatment given here is similar to that presented by Zakroczymski [4], but differs somewhat in detail. Zakroczymski's treatment is given exclusively for a uniform initial hydrogen distribution in the cylinder while the present method deals with either uniform or non-uniform distributions. If the cylindrical medium is of radius a and the boundary conditions are

$S = 0$  at  $r = a$  for all  $t$

$C = f(r)$  for  $a < r < 0$  at  $t = 0$

the general solution is

$$C(r) = \frac{2}{a^2} \sum_1^{\infty} e^{-D\alpha_n^2 t} \frac{\int_0^a r f(r) J_0(\alpha_n r) dr}{[J_0'(\alpha_n a)]^2} J_0(\alpha_n r) \quad (6)$$

Values of  $C(r)$  at 10,000 and 50,000 seconds, as calculated by the above equation for an Incoloy 903 cylinder, are shown in Figure (1). As seen from this illustration, the desorption process is characterized by a peak, the maximum of which decreases in amplitude and moves inward with increasing time, the hydrogen distribution thus becoming more uniform.

In equation (6)  $f(r)$  may be calculated from equation (1) or, if a uniform initial distribution is the case, then  $f(r) = C_0$ .

The amount of hydrogen  $Q(t)$  which has diffused out of the cylindrical medium per unit length after time  $t$  is

$$Q(t) = Q_{HM}^{\infty} - 2\pi \int_0^a C(r) r dr \quad (7)$$

After a long time, values of  $C(r)$  are given by the first term of equation (6). Then

$$C(r) = \frac{2}{a^2} \frac{\int_0^a r f(r) J_0(\alpha_1 r) dr}{[J_0'(\alpha_1 a)]^2} J_0(\alpha_1 r) e^{-t/\tau} \quad (8)$$

where  $\tau = 1/\alpha_1^2 D = a^2/2.405^2 D$ . Then equation (7) may be written

$$Q(t) = Q_{HM}^{\infty} - Ae^{-t/\tau} \quad (9)$$

where  $A$  is given by the appropriate substitution of equation (8) into equation (7). The desorption current at time  $t$  is given by the differentiation of equation (9) with respect to time.



$$I(t) = \frac{A}{\tau} e^{-t/\tau} \quad (10)$$

or

$$\log I(t) = \log \alpha + \beta t \quad (11)$$

where  $\alpha = A/\tau$  and  $\beta = -1/2.303\tau$  so that  $A = -0.434216 \alpha/\beta$ . It can also be shown that  $D = -0.398 a^2\beta$ . Equation (9) provides a means for extrapolating the hydrogen desorption to infinite time and thus to obtain  $Q_{HM}^\infty$ , the total coulombs of hydrogen initially present in the sample. The initial hydrogen concentration  $C_0$  is given by

$$C_0 = Q_{HM}^\infty/\pi a^2 \quad (12)$$

In practice, to obtain curves for the amount of hydrogen desorbed versus time the following equation is used.

$$Q(t) = Q_{HM}^\infty - 0.6015146 d \int_0^a rC(r)dr \quad (13)$$

Here, the factor 0.6015146 is necessary to convert ppm-cm<sup>2</sup> to coulombs and  $d$  is the metal density.  $Q_{HM}^\infty$  is first determined through integration of the observed experimental curve to  $t = t_{\max}$  for the experiment and extrapolating to infinite time using equation (9).

## NUMERICAL SOLUTION WITH PDEONE

The Fortran program PDEONE was developed by Sincovec and Madsen [3] and also reported by Murphy [5]. In general, it solves the following set of coupled nonlinear parabolic equations with nonlinear boundary conditions:

$$\frac{\delta u_k}{\delta t} = f_k \left[ t, x, u_1, u_2, \dots, u_n, \frac{\delta u_1}{\delta X_1}, \frac{\delta u_2}{\delta X_2}, \dots, \frac{\delta u_n}{\delta X_n} \right. \\ \left. \frac{1}{X^c} \frac{\delta}{\delta X} \left( X^c D_{k,1} \delta u_1 \right), \frac{1}{X^c} \frac{\delta}{\delta X} \left( X^c D_{k,2} \frac{\delta u_2}{\delta X} \right), \dots, \frac{1}{X^c} \frac{\delta}{\delta X} \left( X^c D_{k,n} \frac{\delta u_n}{\delta X} \right) \right] \quad (14)$$

for  $a < x < b$ ,  $t > t_0$ , and  $k = 1, 2, \dots, n$  with the boundary conditions

$$\alpha_k u_k + \beta_k \frac{\delta u_k}{\delta X} = \delta_k \quad \text{at } x = a \quad \text{and } x = b, \quad t > t_0, \quad k = 1, 2, \dots, n$$

and the initial conditions

$$u_k(t_0, X) = \phi_k(X) \quad a \leq x \leq b, \quad k = 1, 2, \dots, n \quad .$$

The power  $c$  is 0, 1, 2, depending on whether the problem is in cartesian, cylindrical, or spherical coordinates. In the case of a cylinder, the boundary conditions for charging are:

$$\alpha = 0, \quad \beta = 1, \quad \text{and } \gamma = 0 \quad \text{at } r = 0 \quad (15)$$

and

$$\alpha = 1, \quad \beta = 0, \quad \text{and } \gamma = S \quad \text{at } r = a \quad (16)$$

For desorption, the boundary conditions are:

$$\alpha = 0, \quad \beta = 1, \quad \text{and } \gamma = 0 \quad \text{at } r = 0 \quad (17)$$

and

$$\alpha = 1, \quad \beta = 0, \quad \text{and } \gamma = 0 \quad \text{at } r = a \quad (18)$$

The program was set up to calculate absorption, desorption, or both as required, with coulombs desorbed versus time being calculated as in the case of the analytical solutions. In the present case, the Jacobian for the problem, as described by Murphy [5], was calculated numerically, the desorption curves with 15 points [equation (13)] being calculated in approximately two minutes with either uniform or non-uniform initial distributions, using an IBM PC/XT computer.

## EXPERIMENTAL

The EG&G-PARC Model 350A corrosion measurement console was employed for all electrochemical measurements in this work. The sample holder is shown in Figure 2. The cylindrical specimens were 2.54 cm long with a radius of 0.3175 cm. Specimens were drilled and tapped at one end to accept a 3-48 thread, as required by the sample holder. All specimens were heat treated to a high strength level, although measurements showed that the strength level made little difference in the hydrogen absorption or desorption characteristics of the metals. Samples were electrolytically charged for one hour at 25°C in 0.1N H<sub>2</sub>SO<sub>4</sub> at a current density of 40 mA/cm<sup>2</sup> for all samples except 4340 (5000) steel, which was charged at 10 mA/cm<sup>2</sup>. Charging of all samples at 150°C, at the same current densities, was carried out in a eutectic mixture of molten NaHSO<sub>4</sub>·H<sub>2</sub>O and KHSO<sub>4</sub> for the same time length.

Sample blanks were run at a constant potential of +0.25V (NHE) in a 0.1N NaOH solution at 25°C. The period of measurement was 150,000 sec of each sample, with the current being measured at 500 sec intervals. Data for hydrogen containing samples were collected in the same manner, with the currents due to hydrogen being obtained through subtraction of the currents for the blanks. After each run, the current versus time data were read to an IBM PC/XT computer. After data from both the hydrogen containing sample and its corresponding blank were obtained, the experimental curve, Q(t) versus time was obtained through integration of the current-time curves. Values of Q<sub>HM</sub>, the observed concentration, and D were obtained according to methods described previously. Values of log α and β, the intercepts and slopes, respectively, of the fit of log I(t) versus t are listed in Table 1 for all samples. The standard errors in β, as obtained from the least squares fit, are about 9 percent of the nominal values on the average, while the standard errors in the values of log α are about 0.5 percent of the nominal values on the average. The observed error in each diffusion coefficient and each value of C<sub>0</sub> obtained by electrochemical means (Table 2) is therefore taken as 10 percent of the calculated value.

Total hydrogen concentrations were determined using a Leco Model RH2 Hydrogen Analyzer. Specimens 1.27 cm long, again with a radius of 0.3175 cm, were charged in the same manner as those for the electrochemical measurements and at the same current densities. Calibration of the Analyzer was accomplished with standard samples, and the error associated with each measurement is approximately 0.20 ppm. Hydrogen concentrations for charged samples were obtained after subtraction of values obtained for uncharged specimens or blanks. Hydrogen concentrations obtained using this method are also listed in Table 2.

For the determination of the lattice constants for several of the metal alloys by X-ray diffraction, flat specimens approximately 1.4 cm in diameter and 0.16 cm thick were polished on one face, and X-ray diffraction patterns were recorded, peak positions corrected with a silicon standard, and the lattice parameters determined using a least squares procedure.

## RESULTS AND DISCUSSION

### General

Representative desorption curves (coulombs desorbed versus time) are shown in Figures 3, 4, and 5. The observed desorption curve for Incoloy 903 (Fig. 3) is fit very closely by the theoretical curve corresponding to a 100 percent non-uniform distribution. In this case, the diffusion coefficient for the absorption of hydrogen is equal to the diffusion coefficient for desorption. A completely different situation is shown in Figure 4 for 18 Ni (250) maraging steel at 150°C. Here, the observed desorption curve is matched most closely by a theoretical curve consisting of a 91.2 percent uniform distribution. In cases of this kind, the diffusion coefficient for hydrogen absorption is much greater than that for desorption, indicating a high affinity of the metal alloy for hydrogen. An intermediate case is illustrated in Figure 5 for 18 Ni (250) maraging steel at 25°C, where the observed desorption curve is matched most closely by a hybrid curve with a 62.6 percent uniform distribution. The degrees of uniformity obtained charging the cylinders at 25°C for each of the metal alloys studied are shown in Table 3 together with the structure type for each alloy and percent iron. The results show that high distribution uniformity is obtained for body centered cubic structures, indicating that hydrogen enters metal alloys with that structure type more readily than it does in the case of face-centered cubic structures. Incoloy 903, which contains 39 percent Fe, shows essentially a non-uniform type hydrogen distribution due to its face-centered cubic atomic arrangement as do all of the remaining nickel base alloys, which are also face-centered cubic. The greater ease of hydrogen penetration in body-centered cubic structures is attributed to a greater number of lattice vacancies present in these structures, as will be discussed later. Curves showing the normalized hydrogen absorption profiles after charging for 1 hr at 25°C are shown in Figure 1340 (6414) steel and Incoloy 903. Lattice constants were obtained for several of the metal alloys by x-ray diffraction, and these are listed in Table 4 along with values for pure iron and nickel. The degrees of uniformity obtained by charging the cylindrical samples at 150°C are shown in Table 5. As the results show, high distribution uniformities are exhibited for all metal alloys charged at this temperature, with an appropriately larger hydrogen diffusion coefficient at the higher temperature. The values of all diffusion coefficients obtained in this work, obtained through desorption measurements at 25°C and 150°C, are listed in Table 6. Agreement is generally good for samples charged at 25°C and 150°C, with a few results differing. Nevertheless, all quantities are the effective values for the corresponding metal alloys.

The effective values of  $D$  for hydrogen absorption at 150°C were obtained in the following way. The hydrogen distribution profiles were calculated according to the values of percent uniformity and initial uniform concentrations and concentration profiles, obtained theoretically using parameters obtained from the desorption curves for 100 percent non-uniform distributions. The resulting curves were then fitted, using equation (1), by the method of least squares, the parameters being the apparent concentration ( $S$ ) and the diffusion coefficient ( $D$ ), as illustrated in Figure 7. The values of  $D_0$  for the Arrhenius equation were then determined by simultaneous solution of the equations at 25°C and 150°C. The values so obtained are listed in Table 7.

## Hydrogen Trapping and Metal Embrittlement

Hydrogen in high strength metals can exist in two forms, namely, trapped or immobile hydrogen and mobile or diffusible hydrogen. In the present work, the EG&G-PARC Model 350A Corrosion Measurement Console was used for determination of the diffusible hydrogen and a Leco Model RH2 Analyzer was used to determine the total hydrogen, the difference being due to trapped hydrogen. The trapped hydrogen does not diffuse and does not contribute to hydrogen embrittlement [6]. Among the postulated causes of hydrogen trapping are microstructural features such as grain boundaries, dislocations, second phase particles, voids, and interstitial solute atoms [7,8,9]. Through the use of electrochemical permeation studies of Fe-Ti-C alloys with varying Ti/C ratios, Pressouyre and Bernstein [7] have characterized Ti substitutional atoms as low occupancy reversible trap sites (low energy traps) for hydrogen. Incoherent TiC particles, on the other hand, were found to be larger occupancy, irreversible trap sites (high energy traps). Since the substitutional sites are low energy traps, both trapping and de-trapping occur more easily than in the case of the TiC particles or high energy traps [9]. For the formation of  $TiH_2$  at room temperature, the thermodynamic driving force,  $\Delta G$ , is negative, but it is not expected that a hydride will form. It is simply an indication that there is no thermodynamic barrier to the reaction. The chemical driving force disappears if titanium is already associated with nitrogen or carbon. Thus, the nature of any attraction between TiC and hydrogen will not be chemical in origin, but will be more of a surface absorption interaction [7]. It is believed also that the attraction between titanium and hydrogen is of electronic origin.

Hydrogen concentrations obtained using both the electrochemical method and the Leco Analyzer are shown in Table 2 for cylindrical specimens charged at 25°C and 150°C. Within the experimental error, there is little or no trapping in any of the metal alloys charged at 25°C. Significant evidence of trapping for samples charged at 150°C occurs in 4340M steel and the nickel base alloys Rene' 41, Incoloy 903, MAR-M-246, Waspaloy, and IN-100. Incoloy 903, which is known to have a very low susceptibility to hydrogen embrittlement [10], has dispersed phases consisting of TiC and of carbides containing both Ti and Nb. The remainder of the nickel base alloys all contain titanium. Also, both Incoloy 903 and IN-100, which contains 4.7 percent Ti, show very high hydrogen concentrations in the samples charged at 150°C. 4340M steel contains about 0.1 percent V, 0.01 percent Ti, which is present in occluded particles, and about 0.4 percent Mo, which are all carbide formers, and these are believed to be responsible for the increased hydrogen trapping and decreased susceptibility to hydrogen embrittlement of 4340M steel [11] as opposed to 4340 (6414) and 4340 (5000) steels.

Hydrogen desorption at 430°F for 4340M steel, Incoloy 903 and IN-100 was determined by baking at that temperature for specified periods of time and measuring the remaining hydrogen concentrations with the Leco Analyzer to determine the total hydrogen contents after baking. It was assumed that the hydrogen desorption followed first order kinetics

$$c(t) = C_0 e^{-kt} \quad (19)$$

where  $c(t)$  is the hydrogen concentration at time  $t$ ,  $C_0$  is the initial hydrogen concentration, and  $k$  is the rate constant for the desorption. The experimental points were fitted to equation (19) using the method of least squares, and the parameters obtained for the three metal alloys are listed in Table 9, along with the

corresponding half-lives for hydrogen desorption. The bulk of the trapped hydrogen was desorbed after about 1 hr, and should be a result of the desorption of reversibly trapped hydrogen and mobile hydrogen. Therefore, the parameters listed in Table 9 correspond mainly to the desorption of irreversibly trapped hydrogen. For comparison, the half life for hydrogen desorption by ordinary 4340 steel is about 20 min on baking at 375°F. Thus, even irreversibly trapped hydrogen is desorbed at higher temperatures, and can provide an internal hydrogen source when the metals are heated. Further, when the trapping sites become saturated with hydrogen on charging, trapping no longer provides protection from hydrogen embrittlement, and the metals again become susceptible to the effects of hydrogen.

### **The Entry of Hydrogen into BCC Metals**

The belief has long existed that hydrogen enters only the grain boundaries of the body-centered cubic (BCC), iron containing steels. The solubility of hydrogen in such metals has been determined as only 0.01 ppm [12]. However, this value was obtained by the gas equilibration method, where the solubility is strongly dependent on the pressure, the value of which was not reported. Results of the present work, in the case of the 4340 steels, indicate that hydrogen is more likely to enter the solid granular particles rather than grain boundaries. The charging current for 4340 (5000) steel, which has large grains, was one-fourth that for the 4340 (6414) and 4340M steels, which are composed of small grains. However, about the same hydrogen concentrations were obtained in all three cases. This indicates that as the grain size to grain boundary area increases, the solubility of hydrogen in the metal becomes greater and that hydrogen preferentially enters the grain bodies rather than the grain boundaries. Also, the ability of pure iron single crystals to absorb hydrogen when electrolytically charged was determined, and the result is listed in Table 2. The hydrogen concentration obtained on charging is comparable to the concentrations obtained for all other metals charged at 25°C. Also, the single crystals, as obtained, contained approximately 3 ppm of deeply trapped hydrogen which had to be removed by baking at high temperature before the charging experiments could be performed. Thus, the results of the present work do not support the contention that hydrogen primarily enters the grain boundaries of iron or other BCC metals.

### **The Interaction of Hydrogen with Metals**

The material in this section is not primarily a result of information obtained in the present experimental work, but is based mostly on the work of other investigators. However, it is included for completeness. It has been shown that nickel films could be electrolytically charged with hydrogen to concentrations as high as 0.7 hydrogen atoms per nickel atom [13]. Wollan et al. [14] have shown, using neutron diffraction, that the hydrogen atoms occupy the face centers, or octahedral positions, of the face-centered cubic (FCC) nickel metal lattice. Further, the entry of hydrogen into the metal is accompanied by a 6 percent increase in the Ni lattice parameter or an 18 percent volume increase. Further, changes in magnetic properties on hydrogen uptake are observed, suggesting electron transfer and interaction of hydrogen with the metal. In Ni, the holes in the d-shell are assumed to occupy the t-orbitals which have strong overlap with near neighbor atoms. As a result, the electrons from the hydrogen atoms would be shared with or transferred to the Ni atoms, suggesting a possible ionic structure of the type  $\text{Ni}^-\text{H}^+$  (or  $\text{Ni}^+\text{H}^-$ ). This idea has been supported by other investigators [15]. Further, the electron transfer is reversible, since the so-called nickel hydride is unstable. Nevertheless, the interaction of the electrons of hydrogen atoms with the Ni atoms results in a weakening of the metallic bond and very likely is the ultimate cause of hydrogen embrittlement.

The hydrogen atoms in the Ni lattice are each surrounded by six Ni atoms at a distance of 1.87 Å in the expanded lattice, and the end result is a NaCl type structure which has a lattice energy of -330 kcal per gram atom of Ni. This energy is very likely the driving force for the interaction of hydrogen and Ni to cause embrittlement, since it can be shown that the overall energy change, including ionization of hydrogen atoms to ions, is negative and therefore thermodynamically possible. If electron transfer is only partial, the energy change is proportionately less, but still negative. It is assumed in the foregoing considerations that the hydrogen bond is broken by electrolytic means in electrolyte charging and through molecular collisions and thermal dissociation in the case of high pressure charging. A view of the NaCl lattice is shown in Figure 8.

In the case of iron, investigations have concluded that the hydrogen atoms occupy the so-called tetrahedral positions in the iron lattice which is body-centered cubic [16,17]. However, tetrahedra are not present in this structure, but the structure element referred to is really pyramidal in nature. Also, on careful examination of spatial requirements, considering both the radii (including the Van der Waal's radius for H) of Fe and H atoms or ions, the only conclusion which can be reached is that the hydrogen atoms (or ions) occupy the face centers of the cubic lattice. There are, therefore, 1.5 such sites per Fe atom as compared to only 1 site per Ni atom in the FCC structure. This may be the reason that hydrogen diffuses more quickly through the BCC lattices on charging at 25°C, as indicated by the experimental results of the present work. In the bipyramidal arrangement, each hydrogen atom is surrounded by 4 Fe atoms at a distance of 2.02Å and 2 Fe atoms at a distance of 1.43Å. This structure, commonly known as the Perovskite structure, is shown in Figure 9. The shortest value of the equilibrium distance ( $r_e$ ) in gaseous Fe-H, as obtained from spectroscopic data [18], is 1.476Å, so that a slight expansion of the lattice might occur, but has never been observed. The crystal lattice energy of this type lattice is -1437 kcal per mole of Fe<sub>2</sub>H<sub>3</sub>. Considerations, similar to those made in the case of Ni, show that the energy change is much more negative in the case of BCC metals, which might explain why such structures are more highly susceptible to hydrogen embrittlement.

## CONCLUSIONS

The employment of the present electrochemical method along with fusion methods seems to be a feasible way to study trapping in metal alloys. The mobile or diffusible hydrogen is determined with the electrochemical method and the total hydrogen by a fusion technique, the difference in hydrogen concentrations so obtained being due to trapped hydrogen. The results of the present study are consistent with those from other studies, in which it was found that trapping depended on Ti content, as well as the presence of other carbide formers, with both reversible and irreversible trapping of hydrogen taking place. The present work indicates that trapping is less extensive at 25°C than at higher temperatures. The metals or metal carbides can become saturated with hydrogen, after which they become ineffective for lowering the susceptibility of the parent metal to hydrogen embrittlement. Also, these traps can act as internal sources for hydrogen release at higher temperatures.

It has been found that hydrogen entry into the BCC 4340 steels takes place preferentially through the grain bodies rather than through grain boundaries, contrary to present day beliefs. Also the hydrogen solubilities in the structures with large grain diameters are much greater than those with smaller grains in the 4340 steels, the required charging conditions to obtain the same hydrogen concentration being much less in 4340 (5000) steel, with large grain diameters, than in 4340 (6414) and 4340M steels, which are made up of small grains.

Further evidence that hydrogen atoms may occupy the bipyramidal sites in the BCC lattice was provided through the electrolytic charging of Fe single crystals, where hydrogen concentrations comparable to those for other metals were obtained.

In addition, the electrochemical work shows that hydrogen penetrates the BCC cubic lattice much more readily than the FCC lattice, there being 1.5 possible sites for hydrogen per metal atom in the BCC lattice, whereas there is only one in the FCC lattice. Further, the calculation of lattice energies for both BCC and FCC ionic lattices indicates that these may be the driving forces for the interaction of hydrogen with metals, leading to hydrogen embrittlement. The total energy change is more negative for the BCC lattice than for the FCC lattice on hydrogen entry and may be the reason for the greater hydrogen embrittlement susceptibility of these materials.

Finally, the agreement of the hydrogen concentrations obtained by the electrochemical method at 25°C, where hydrogen trapping is not a factor, with those obtained using the fusion technique, along with the agreement of these measurements with diffusion theory, provides strong evidence for the validity and power of the present electrochemical method. A review of the diffusion theory presented previously shows also that the values of the hydrogen diffusion coefficients obtained with the present electrochemical method are intimately related to the value of the observed hydrogen concentrations. Therefore, the agreement of these concentrations with those for the fusion method at 25°C also provides evidence for the validity of the values for hydrogen diffusion coefficient obtained with the electrochemical method.



## REFERENCES

1. Danford, M. D.: NASA Technical Paper 2459, April 1985.
2. Barrer, R. M.: Diffusion in and Through Solids. Cambridge, 1941.
3. Sincovec, R. F. and Madsen, N. K.: ACM Trans. Math. Software, Vol. 1, 1975, pp. 232-60.
4. Zakroczymski, T.: Corrosion, Vol. 38, 1982, p. 218.
5. Murphy, W. D.: Rockwell International Science Center Internal Report SC-DIT-76-10, 1976.
6. Townsend, H. E.: Corrosion, Vol. 37, 1981, p. 115.
7. Pressouyre, G. M. and Bernstein, I. M.: Metallurgical Trans., Vol. 9A, 1978, p. 1571.
8. Stevens, M. F. and Bernstein, I. M.: Metallurgical Trans., Vol. 16A, 1985, p. 1879.
9. Lee, J. and Lee, S. M.: Paper presented at the International Symposium on Hydrogen in Metals, Belfast, U.K., March 26-29, 1985.
10. Drinan, D. T., private communication.
11. Raymond, L.: Study of Effects of Alloying and Heat Treatment on Hydrogen Embrittlement Susceptibility of Electroslag Remelted 4340 Steel, Contract DAAG46-85-C-0020, U.S. Army Materials Laboratory, October 1986.
12. Kiuchi, K. and McClellan: Acta Metall., Vol. 31, 1983, p. 961.
13. Baranowski, B. and Smialowski, M.: J. Phys. Chem. Solids, Vol. 12, 1959, p. 206.
14. Wollan, E. O., Cable, J. W., and Koehler, W. C.: J. Phys. Chem. Solids, Vol. 24, 1963, p. 1141.
15. Oriani, R. A.: Proceedings of Conference on Fundamental Aspects of Stress Corrosion Cracking, R. W. Staehle, ed., Ohio State University, 1967, p. 32.
16. Seeger, A.: Phys. Lett., Vol. A58A, 1976, p. 137.
17. Wallace, J. P.: Scripta Metall., Vol. 12, 1978, p. 791.
18. Herzberg, G.: Spectra of Diatomic Molecules, D. Van Nostrand Company, Inc., New York, 1950.

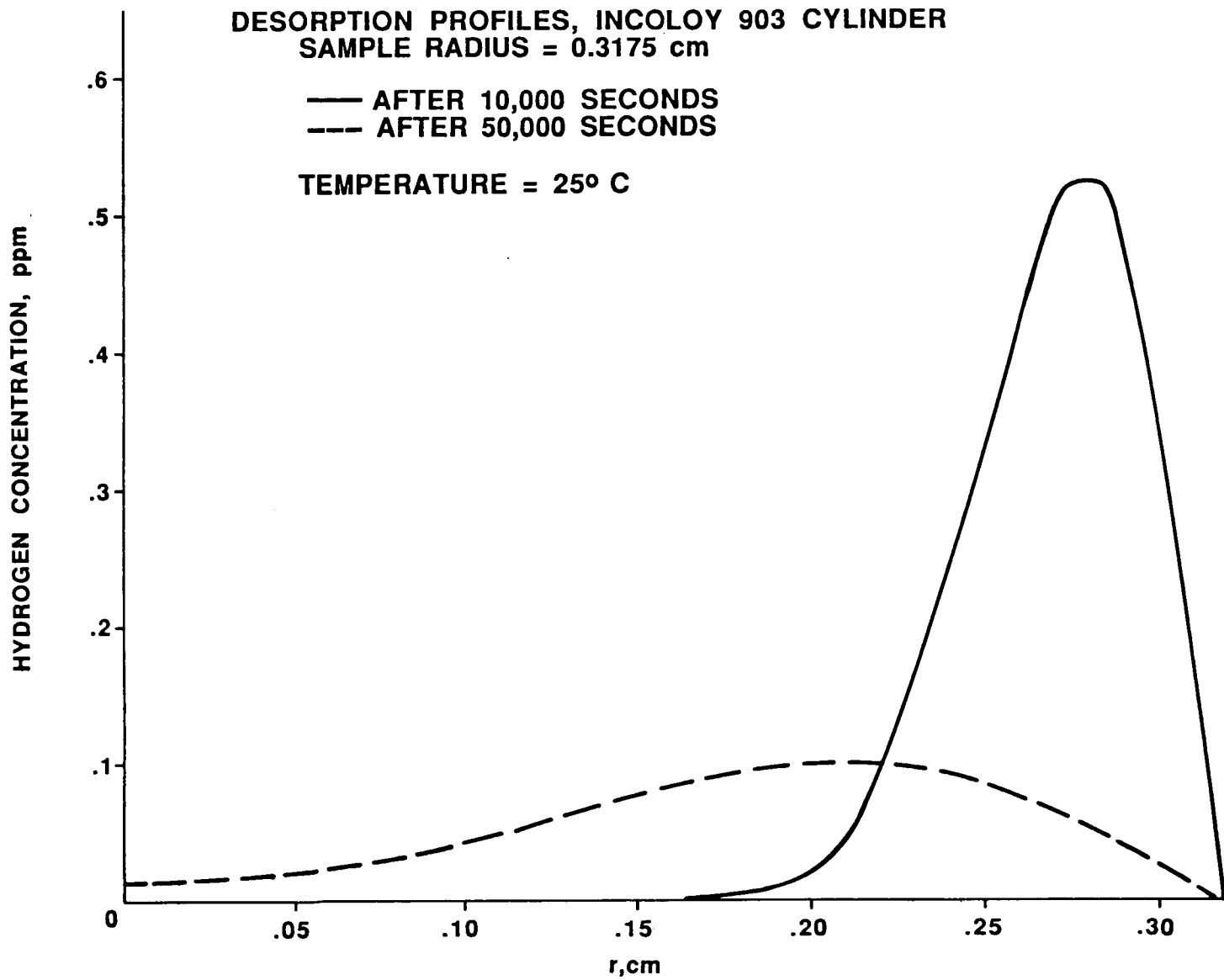


Figure 1. Desorption profiles for Incoloy 903 cylinders.

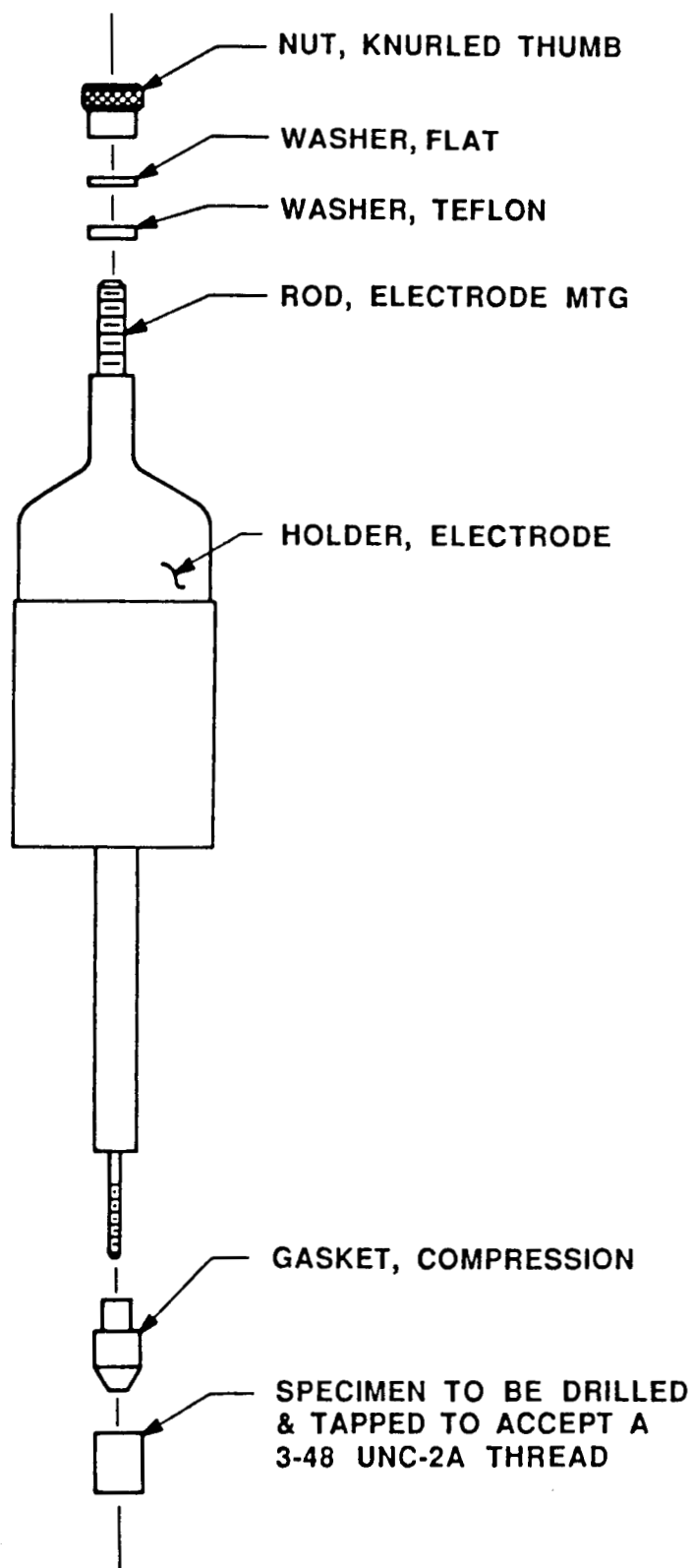


Figure 2. Exploded view of the sample holder.

HYDROGEN DESORPTION, INCOLOY 903  
 ● THEORETICAL CURVE, UNIFORM INITIAL DISTRIBUTION  
 — THEORETICAL CURVE, NON-UNIFORM INITIAL DISTRIBUTION  
 ○ EXPERIMENTAL CURVE

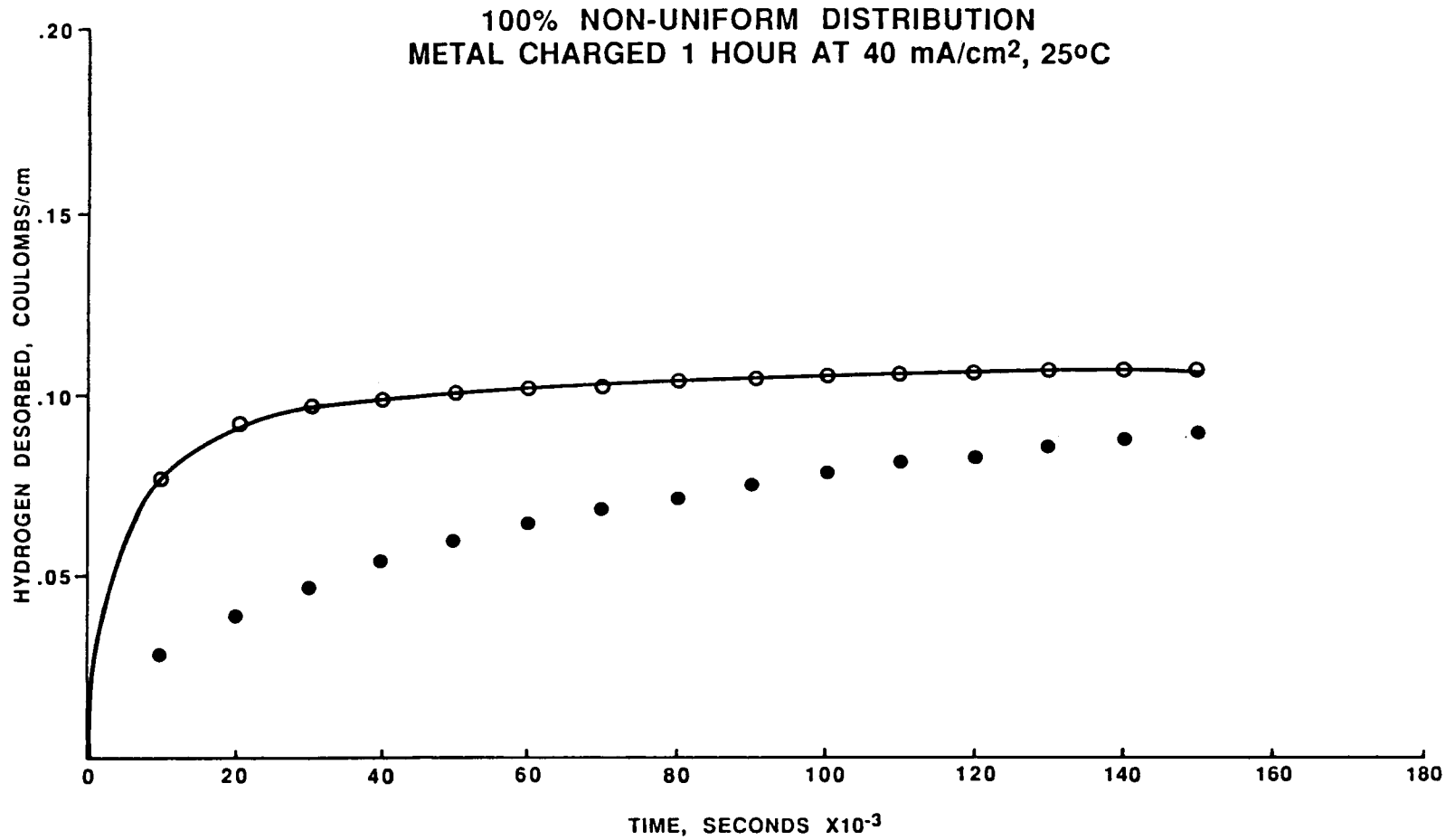


Figure 3. Theoretical and experimental desorption curves for an Incoloy 903 cylinder charged at 25°C.

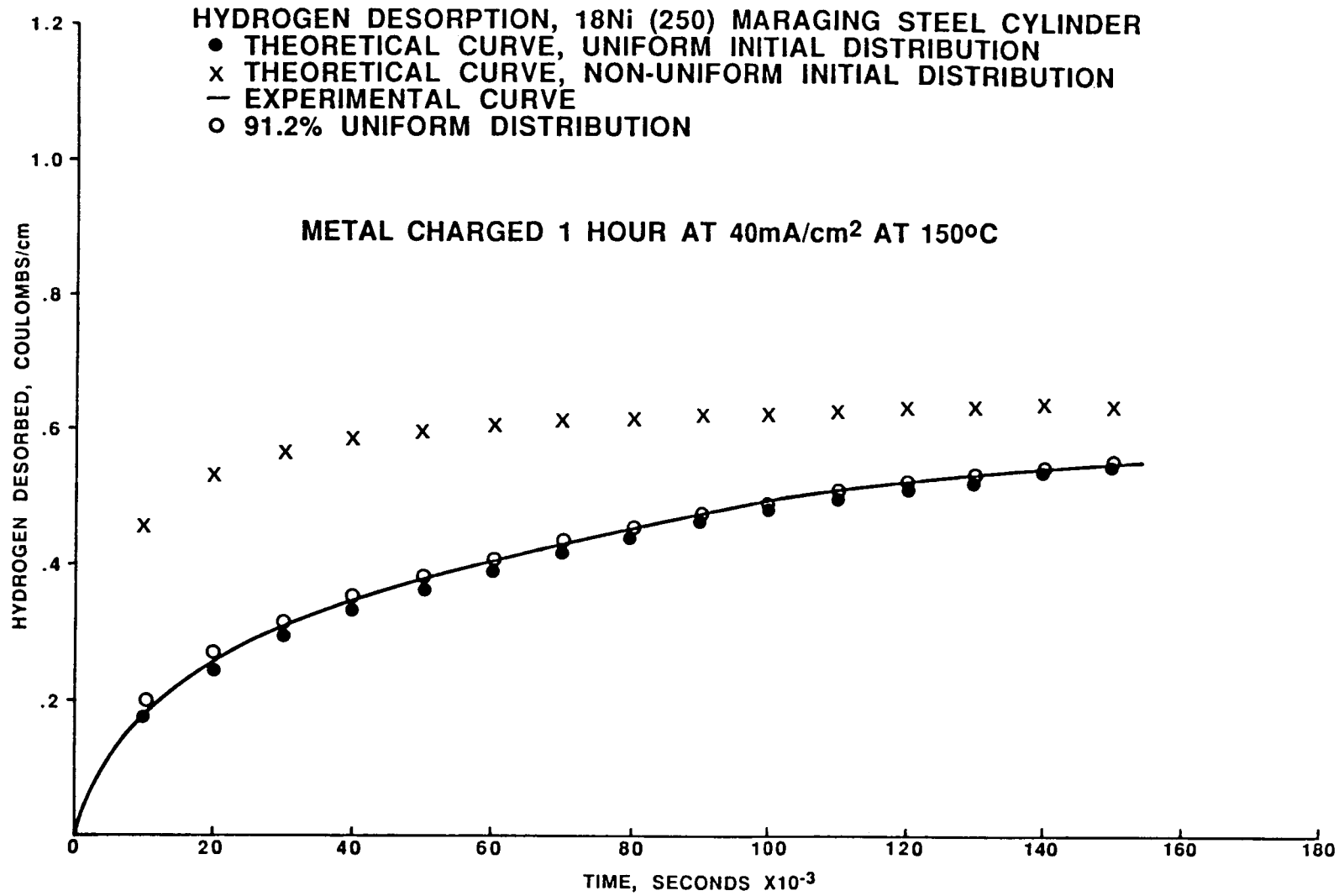


Figure 4. Theoretical and experimental desorption curves for an 18 Ni (250) maraging steel cylinder charged at 150°C.

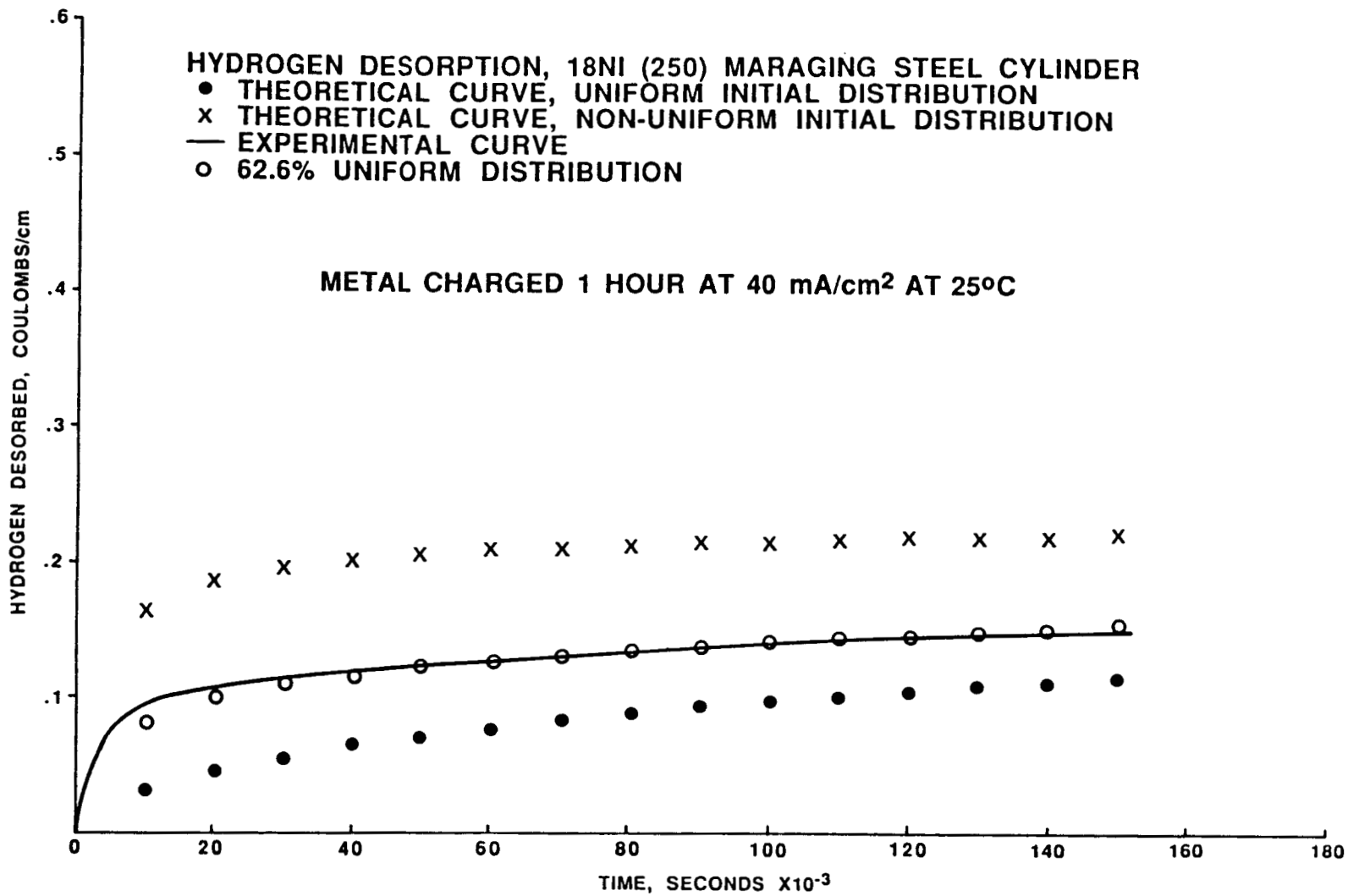


Figure 5. Theoretical and experimental desorption curves for an 18 Ni (250) maraging steel cylinder charged at 25°C.

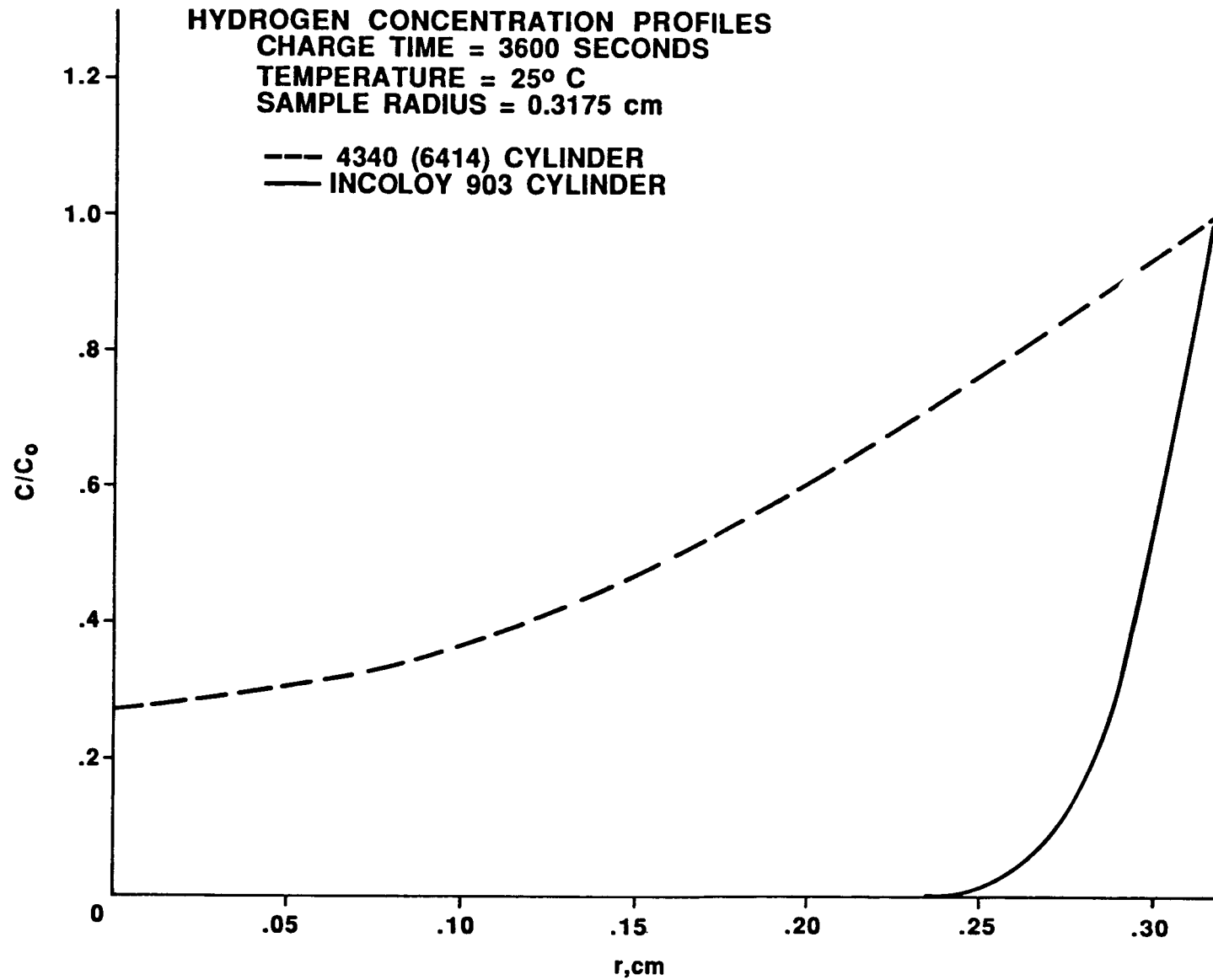


Figure 6. Theoretical absorption profiles for 4340 (6414) and Incoloy 903 cylinders charged at 25°C.

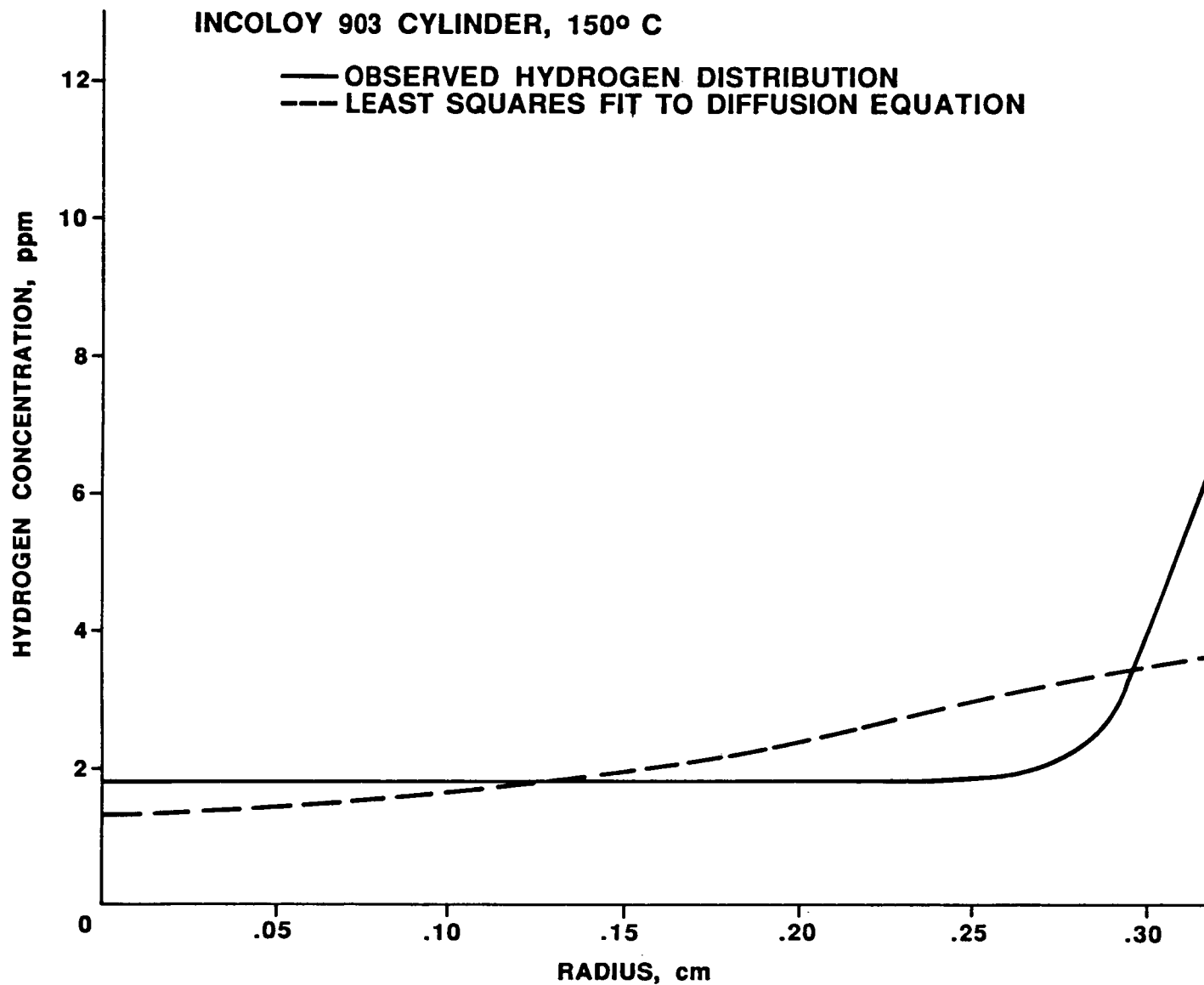


Figure 7. Least squares fit of observed hydrogen distribution with diffusion equation for an Incoloy 903 cylinder charged at 150°C.



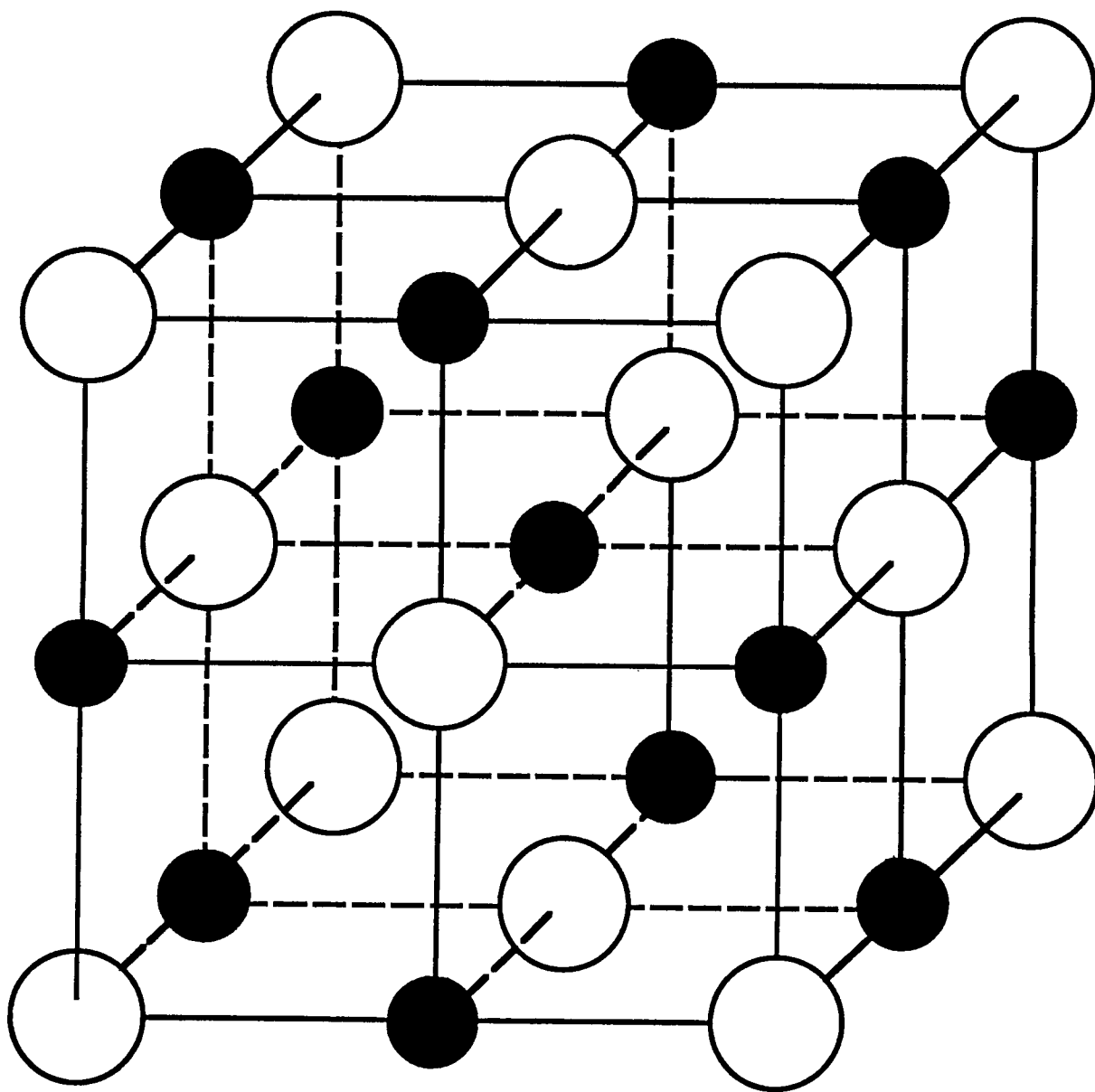


Figure 8. The hypothetical structure of NiH (NaCl structure).  
Positions of H atoms are designated by open circles.

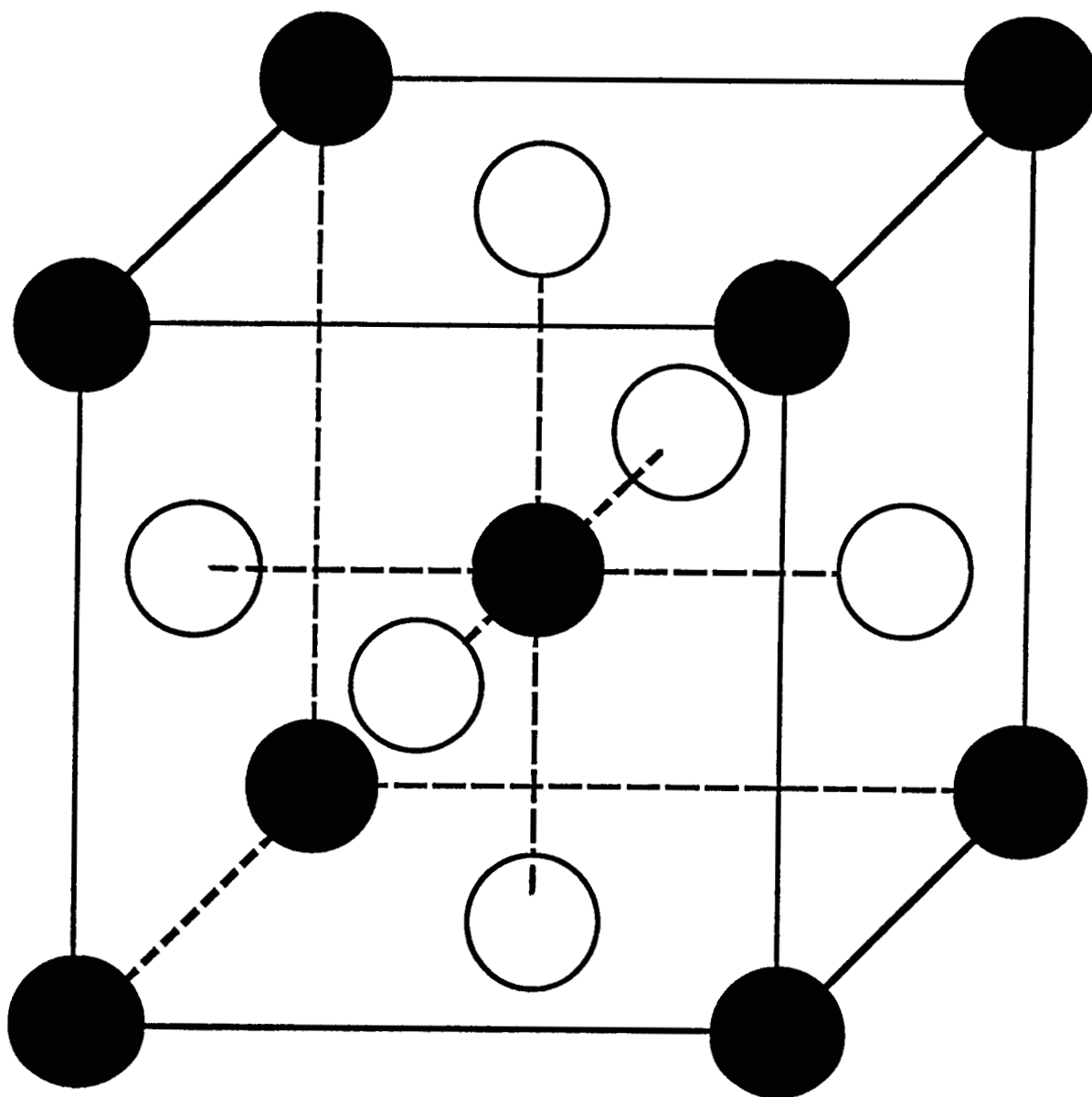


Figure 9. The hypothetical structure of Fe<sub>2</sub>H<sub>3</sub> (Perovskite structure).  
Positions of H atoms are designated by open circles.

TABLE 1. VALUES OF  $\beta$  AND LOG  $\alpha$  OBTAINED BY LEAST SQUARES FIT OF OBSERVED DATA

Material	T (°C) <sup>a</sup>	$-\beta \times 10^6$	Std. Error	$-\text{Log } \alpha \times 10^6$	Std. Error
4340(500)	25	6.51067	0.16741	5.7475	0.0196
	150	5.99156	0.08499	5.5609	0.0100
4340 (6414)	25	1.45455	0.21974	6.5547	0.0258
	150	0.83280	0.20695	6.5103	0.0243
4340M	25	4.05486	0.96709	5.9871	0.1169
	150	4.11706	0.17029	5.6897	0.0200
18 Ni (250) MS	25	1.03104	0.26936	6.5358	0.0316
	150	3.94114	0.05677	5.4117	0.0067
Incoloy 903	25	3.63176	0.28796	6.8583	0.0338
	150	2.14527	0.28161	5.7218	0.0330
Waspaloy (TMP)	25	4.98886	0.47124	6.4956	0.0553
	150	2.37370	0.23344	6.1919	0.0274
Waspaloy (Lad)	25	5.52162	0.21854	6.5079	0.0256
	150	4.47948	0.45522	5.7775	0.0534
Rene' 41	25	4.31896	0.04302	6.4546	0.0050
	150	3.81276	0.38157	6.1429	0.0447
MAR-M-246	25	3.65890	0.21911	6.5482	0.0257
	150	4.74060	0.24640	5.9411	0.0289
IN-100	25	4.48599	0.48599	6.2887	0.0570
	150	2.19885	0.07399	5.8359	0.0087

a. Charging temperature. Desorption is measured at 25°C.

TABLE 2. HYDROGEN CONCENTRATIONS IN METALS CHARGED ELECTROLYTICALLY AT 25°C AND 150°C

Material	T(°C)	Electrochemical Method	Leco Analyzer
4340 (5000) <sup>a</sup>	25	1.03 ± 0.10	1.10 ± 0.20
	150	1.29 ± 0.13	1.05 ± 0.20
4340 (6414) <sup>b</sup>	25	0.79 ± 0.08	0.81 ± 0.20
	150	1.12 ± 0.11	1.12 ± 0.20
4340M	25	0.73 ± 0.07	1.01 ± 0.20
	150	1.33 ± 0.13	2.56 ± 0.20
Rene' 41	25	1.03 ± 0.10	1.11 ± 0.20
	150	0.47 ± 0.05	2.46 ± 0.20
Incoloy 903	25	0.72 ± 0.07	0.57 ± 0.20
	150	2.28 ± 0.24	5.34 ± 0.20
MAR-M-246	25	0.66 ± 0.07	0.67 ± 0.20
	150	0.70 ± 0.07	1.85 ± 0.20
MAR-M-246 <sup>d</sup>	25	—	0.53 ± 0.20
	150	—	2.16 ± 0.20
Waspaloy (TMP)	25	0.62 ± 0.06	0.57 ± 0.20
	150	0.79 ± 0.08	1.81 ± 0.20
Waspaloy (Lad) <sup>c</sup>	25	0.56 ± 0.06	0.69 ± 0.20
	150	0.99 ± 0.10	1.53 ± 0.20
18NI(250)MS	25	0.96 ± 0.10	0.53 ± 0.20
	150	2.74 ± 0.28	2.98 ± 0.20
Fe <sup>d</sup>	25	—	0.44 ± 0.20
IN-100	25	1.00 ± 0.10	1.13 ± 0.20
	150	2.05 ± 0.21	6.11 ± 0.20

- a. Air melted material, large grains. Charged at 10 mA/cm<sup>2</sup>.  
All other specimens in this table were charged at 40 mA/cm<sup>2</sup>.
- b. Vacuum melted aerospace material, small grain size.
- c. Waspaloy manufactured by Ladish.
- d. Single crystals.

TABLE 3. HYDROGEN DISTRIBUTION UNIFORMITIES IN  
CYLINDERS CHARGED AT 25°C

Material	Percent Fe	Structure Type <sup>a</sup>	Percent Uniformity
4340 (5000)	96.8	BCC	69.1
4340 (6414)	96.8	BCC	50.7
4340M	96.8	BCC	82.5
18Ni(250)MS	68.0	BCC	63.0
Incoloy 903	39.0	FCC	4.5
Waspaloy (TMP)	2.0	FCC	3.3
Waspaloy (Lad) <sup>b</sup>	0.93	FCC	0.0
Rene' 41	1.09	FCC	0.0
Mar-M-246	0.0	FCC	0.0
IN-100	<0.6	FCC	3.5

a. BCC = body centered cubic; FCC = face centered cubic.

b. Waspaloy manufactured by Ladish.

TABLE 4. STRUCTURE TYPES AND UNIT CELL PARAMETERS FOR METAL ALLOYS

Material	Percent Fe	Percent Ni	Unit Cell Type <sup>a</sup>	a, Å
Fe	100.0	0.0	BCC	2.86
4340 Steel	96.8	2.0	BCC	2.87
18Ni(250)MS	68.0	18.0	BCC	2.87
Incoloy 903	38.0	39.0	FCC	3.60
Rene' 41	<0.3	55.0	FCC	3.60
Waspaloy	2.0	57.0	FCC	3.58
Ni	0.0	100.0	FCC	3.52

a. BCC = body centered cubic; FCC = face centered cubic.

TABLE 5. HYDROGEN DISTRIBUTION UNIFORMITIES IN CYLINDERS CHARGED AT 150°C

Material	Percent Fe	Structure Type <sup>a</sup>	Percent Uniformity
4340 (5000)	96.8	BCC	86.0
4340 (6414)	96.8	BCC	71.7
4340M	96.8	BCC	94.1
18Ni(250)MS	68.0	BCC	91.2
Incoloy 903	39.0	FCC	80.1
Waspaloy (TMP)	2.0	FCC	82.9
Waspaloy (Lad) <sup>b</sup>	0.93	FCC	91.3
Rene' 41	1.09	FCC	97.0
Mar-M-246	0.0	FCC	58.5
IN-100	<0.6	FCC	76.5

a. BCC = body centered cubic; FCC = face centered cubic.

b. Waspaloy manufactured by Ladish.

TABLE 6. VALUES OF DIFFUSION COEFFICIENTS  
OBTAINED FOR VARIOUS ALLOYS

Material	Charging Temperature, (Degrees Centigrade)	D(25°C) × 10 <sup>7</sup> , (cm <sup>2</sup> /sec)
4340(5000)	25	2.61 <sup>a</sup>
	150	2.40
4340(6414)	25	1.63
	150	1.65
4340M	25	0.58
	150	0.33
18Ni(250)MS	25	0.41
	150	1.58
Incoloy 903	25	0.93
	150	0.55
Waspaloy (TMP)	25	2.00
	150	0.95
Waspaloy (Lad)	25	2.22
	150	1.80
Rene' 41	25	1.73
	150	1.53
MAR-M-246	25	1.47
	150	1.90
IN-100	25	5.14
	150	0.88

a. The standard error for each D is about 10 percent of the nominal value.

TABLE 7. VALUES OF  $D_0$  AND E FOR THE ARRHENIUS EQUATION,  $D = D_0 \exp(-E/RT)$

Material	$D_0$ ( $\text{cm}^2/\text{sec}$ )	E (cal/g.atom)
4340(5000)	4.1	7,194
4340(6414)	0.24	9,029
4340M	0.11	7,954
18Ni(250)MS	2.7	10,663
Incoloy 903	0.04	7,715
Waspaloy (TMP)	0.19	8,593
Waspaloy (Lad) <sup>a</sup>	0.12	7,963
Rene' 41	0.39	8,668
MAR-M-246	0.02	6,954
IN-100	0.04	7,730

a. Waspaloy manufactured by Ladish.

TABLE 8. RELATION OF HYDROGEN TRAPPING TO TITANIUM CONTENT AND TEMPERATURE

Material	Percent Ti	Percent Trapping at 25°C <sup>b</sup>	Percent Trapping at 150°C
4340(5000)	0.0	0.0	0.0
4340(6414)	0.0	0.0	0.0
4340M	0.01	0.0	48.0
Rene' 41	3.2	0.0	80.9
Incoloy 903	1.9	0.0	57.3
MAR-M-246	1.5	0.0	62.2
Waspaloy (TMP)	3.0	0.0	56.4
Waspaloy (Lad) <sup>a</sup>	3.0	0.0	35.3
18Ni(250)MS	0.4	0.0	0.0
IN-100	4.7	0.0	66.4

a. Waspaloy manufactured by Ladish.

b. Within the experimental error.



TABLE 9. VALUES OF  $C_o$ , RATE CONSTANT, AND HALF-LIFE OBTAINED ON BAKING AT 221°C (430°F)

Material	$C_o$ , ppm	$k$ (hr <sup>-1</sup> )	$t_{1/2}$ (hr)
4340M	0.70	0.0503	13.8
Incoloy 903	0.54	0.0785	8.8
IN-100	0.35	0.1694	4.1

1. REPORT NO. NASA TP-2744		2. GOVERNMENT ACCESSION NO.		3. RECIPIENT'S CATALOG NO.	
4. TITLE AND SUBTITLE Hydrogen Trapping and the Interaction of Hydrogen With Metals				5. REPORT DATE July 1987	
				6. PERFORMING ORGANIZATION CODE	
7. AUTHOR(S) Merlin D. Danford				8. PERFORMING ORGANIZATION REPORT #	
9. PERFORMING ORGANIZATION NAME AND ADDRESS George C. Marshall Space Flight Center Marshall Space Flight Center, Alabama 35812				10. WORK UNIT NO. M-563	
				11. CONTRACT OR GRANT NO.	
12. SPONSORING AGENCY NAME AND ADDRESS National Aeronautics and Space Administration Washington, D.C. 20546				13. TYPE OF REPORT & PERIOD COVERED  Technical Paper	
				14. SPONSORING AGENCY CODE	
15. SUPPLEMENTARY NOTES Prepared by Materials and Processes Laboratory, Science and Engineering Directorate.					
16. ABSTRACT  A method has been developed for the determination of trapped hydrogen in metal alloys. It involves the determination of mobile hydrogen using the electrochemical method and the determination of total hydrogen with the fusion method, the difference in hydrogen concentrations being due to trapped hydrogen.  It has been found that hydrogen enters body-centered cubic structures primarily through the grain bodies rather than through the grain boundaries. Hydrogen also diffuses much more rapidly in body-centered cubic structures on charging than in face-centered cubic structures, the hydrogen distribution being more uniform in nature. The energy necessary to cause hydrogen embrittlement is postulated to arise from the changes in crystal lattice energies brought about through interaction of hydrogen with atoms in the metal lattice. The total energy change is more negative for body-centered cubic structures, believed to be the cause of a greater tendency toward hydrogen embrittlement. Finally, the agreement of hydrogen concentrations obtained at 25°C by the electrochemical method with those obtained by the fusion method are taken as a strong indication of the power and validity of the electrochemical method.					
17. KEY WORDS Hydrogen Embrittlement Hydrogen Trapping Electrochemical Techniques Hydrogen Interaction with Metals			18. DISTRIBUTION STATEMENT Unclassified - Unlimited  Subject Category 26		
19. SECURITY CLASSIF. (of this report) Unclassified		20. SECURITY CLASSIF. (of this page) Unclassified		21. NO. OF PAGES 34	22. PRICE A03